Heparan sulphate binding controls *in vivo* half-life of the HpARI protein family.

Florent Colomb [1], Abhishek Jamwal [2,4], Adefunke Ogunkanbi [1, 3], Tania Frangova [1], Alice R. Savage [1], Sarah Kelly [1], Gavin J Wright [3], Matthew K. Higgins [2,4], Henry J McSorley [1]

The parasitic nematode *Heligmosomoides polygyrus bakeri* secretes the HpARI family, which bind to IL-33, either suppressing (HpARI1 and HpARI2) or enhancing (HpARI3) responses to the cytokine. We previously showed that HpARI2 also bound to DNA via its first Complement Control Protein (CCP1) domain. Here, we find that HpARI1 can also bind DNA, while HpARI3 cannot. Through the production of HpARI2/HpARI3 CCP1 domain-swapped chimeras, DNA-binding ability can be transferred, and correlates with in vivo half-life of administered proteins. We found that HpARI1 and HpARI2 (but not HpARI3) also binds to the extracellular matrix component heparan sulphate (HS), and structural modelling showed a basic charged patch in the CCP1 domain of HpARI1 and HpARI2 (but not HpARI3) which could facilitate these interactions. Finally, a mutant of HpARI2 was produced which lacked DNA and HS binding, and was also shown to have a short half-life in vivo. Therefore, we propose that during infection the suppressive HpARI1 and HpARI2 proteins have long-lasting effects at the site of deposition due to DNA and/or extracellular matrix interactions, while HpARI3 has a shorter half-life due to a lack of these interactions.

Affiliations:

1. Division of Cell Signalling and Immunology, School of Life Sciences, University of Dundee, Dundee, United Kingdom
2. Department of Biochemistry, University of Oxford, South Parks Rd, OX1 3QU, Oxford, United Kingdom
3. Department of Biology, Hull York Medical School, York Biomedical Research Institute, University of York, York, United Kingdom.
4. Kavli Institute of Nanoscience Discovery, Dorothy-Crowfoot Hodgkin Building, University of Oxford, South Parks Rd, OX1 3QU

IL-33 is a pleiotropic cytokine. It can act as a potent inducer of type 2 immune responses, and genetic studies show a strong link between the IL-33 pathway and the risk of developing allergic asthma (Moffatt et al., 2010; Oboki et al., 2010). Likewise, IL-33 responses are important for induction of anti-parasite type 2 immune responses in helminth infections (McSorley & Smyth, 2021). Conversely, IL-33 is a potent inducer of IFN-γ and regulatory T cell responses, dependent on the cytokine's context, cytokine release mode, and the cell responding to the cytokine (Bonilla et al., 2012; Schiering et al., 2014). Thus, IL-33 can have pro-allergic, pro-inflammatory or anti-inflammatory activities, and modulation of IL-33 responses can have a range of effects.

Parasitic helminths secrete an array of immunomodulatory proteins which tailor the host immune response to allow parasite persistence without immunopathology (Maizels et al., 2018). Our previous work identified the HpARI protein family, secreted by the murine intestinal nematode *Heligmosomoides polygyrus bakeri* (Hpb). Each member of the HpARI family consists of 3 complement control protein domains, CCP1-3 (Colomb et al., 2024). Our initial characterisation of the HpARI protein (later renamed HpARI2) showed that it bound directly to IL-33, inhibiting the interaction between IL-33 and its receptor (Osbourn et al., 2017). Our recent structural characterisation of the HpARI2:IL-33 complex showed that HpARI2 binds IL-33 via interactions between the cytokine and the CCP2 and CCP3 domains of HpARI2. In particular, a long loop in CCP3 contacts IL-33 at a site which overlaps with the IL-33:ST2 binding site, thus inhibiting cytokine-receptor interactions to effectively block the cytokine (Jamwal et al., 2023). However, the CCP1 domain was not characterised in this structure.

We previously showed that HpARI2 can interact with DNA in a non-sequence-specific manner, via its CCP1 domain. Truncations of HpARI2 which lack CCP1 cannot bind to DNA (Osbourn et al., 2017), while HpARI2 truncations lacking the CCP3 domain can still bind to IL-33 (albeit with lower affinity), but cannot block interactions between IL-33 and its receptor (Chauche et al., 2020; Jamwal et al., 2023). Thus, through CCP1-DNA and CCP2/3-IL-33 interactions, HpARI2 binds to genomic DNA and IL-33 within the nucleus of necrotic epithelial cells, tethering the cytokine and preventing its release (Osbourn et al., 2017). Characterisation of the other members of the HpARI family showed that HpARI1, like HpARI2, blocked responses to IL-33. HpARI3, however, bound to IL-33 but did not block interaction of IL-33 with its receptor. Instead HpARI3 stabilised IL-33, amplifying responses to the cytokine in vivo (Colomb et al., 2024). Thus *Hpb* produces a family of structurally similar HpARI molecules with opposing physiological effects.

Here, we investigated the role of the CCP1 domain of the HpARI proteins, and found that HpARI1 and HpARI2 can also bind to heparan sulphate via their CCP1 domain, while HpARI3 cannot. This extracellular matrix binding extends the half-life of HpARI2 *in vivo* at the site of administration.

Results:

HpARI1 and HpARI2 bind to DNA, while HpARI3 does not

HpARI2 was previously shown to tether IL-33 in necrotic cell nuclei (Osbourn et al., 2017). Using a short-term in vivo model of IL-33 release, we co-administered HpARI1, HpARI2 or HpARI3 with Alternaria allergen (Fig 1A) and assessed IL-33 release. As shown previously (Osbourn et al., 2017), due to interaction between the HpARIs and IL-33, released IL-33 could not be detected by ELISA in the presence of HpARIs (Fig 1B). However, denaturing western blots dissociated the HpARI-IL-33 complex and allowed measurement of released IL-33 (Fig 1C and Fig 1 Supplement 1). As shown previously, HpARI2 suppressed the release of IL-33 measured by western blot, due to its tethering function (Osbourn et al., 2017). HpARI1 showed a similar trend which did not reach statistical significance in this experiment. HpARI3 lacked this ability and did not alter the levels of released IL-33 as assessed by western blot. We therefore measured the ability of the HpARIs to bind to DNA (as a correlate of the tethering function of these proteins) using an electromobility shift assay (EMSA) to measure formation of DNA-protein complexes via altered polyacrylamide gel migration of short DNA oligonucleotides. HpARI1 and HpARI2 both caused altered migration of DNA probes, indicating binding to DNA, while HpARI3 did not (Fig 1D). Interestingly, while HpARI2 effectively bound all DNA, HpARI1 showed a reduced DNA-binding ability, only binding 50% of the DNA in this assay (Fig 1E).

The DNA-binding activity of HpARI2 was previously shown to be localised to its CCP1 domain. To assess the stark difference in DNA binding between HpARI2 and HpARI3, fusion constructs were expressed with the CCP1 domain of HpARI2 fused to the CCP2+3 domains of HpARI3 (HpARI2:3) or vice versa (Fig 1F). In EMSA experiments, these constructs showed DNA binding directly related to the source of their CCP1 domain, with HpARI3:2 lacking, and HpARI2:3 showing DNA binding (Fig 1G). Therefore, members of the HpARI family differ in their ability to bind both IL-33 and DNA, the latter of which is mediated solely by the CCP1 domain.

HpARI fusion proteins show unexpected effects on IL-33 responses in vivo

The HpARI2:3 and HpARI3:2 fusion proteins represent useful tools to separate the DNA binding and IL-33 modulation effects of HpARI2 and HpARI3 respectively. These fusion proteins were tested in an in vitro model of IL-33 release and responsiveness (Chauche et al., 2020; Colomb et al., 2024), where the CMT-64 epithelial cell line is freeze-thawed to induce necrosis and IL-33 release in the presence of HpARI proteins. Supernatants from these necrotic cells were then transferred to cultures of bone marrow cells in the presence of IL-2 and IL-7 to support ILC2 differentiation, and IL-33-mediated ILC2 activation was assessed by IL-5 release. As shown previously (Colomb et al., 2024), in this assay HpARI2 dose-dependently suppresses ILC2 responses, while HpARI3 amplifies them (Fig 2A). The HpARI2:3 and HpARI3:2 fusion proteins retained the amplifying or suppressing activities of their CCP2/3 domains. Small alterations in activity were seen when CCP1 domains were swapped, with HpARI2:3 showing decreased activity compared to HpARI3 wild-type (HpARI3 EC50=1.2ng/ml, HpARI3:2 EC50=21.5 ng/ml), and HpARI3:2 showing slightly

117 increased activity compared to HpARI2 wild-type (HpARI2 IC50=1.9 ng/ml, HpARI3:2
118 IC50=1.1 ng/ml).
119
120 As these fusion proteins retained similar activity on IL-33 as their CCP2/3 parent proteins,
121 we then assessed their activity in vivo, first co-administering them with Alternaria allergen
122 and assessing IL-33 release by western blot 15 min later. As expected, HpARI2 and
123 HpARI2:3 tethered IL-33 and reduced its release, due to their combination of IL-33 and
124 DNA binding activities. HpARI3 and HpARI3:2 lack tethering ability, and slightly increased
125 levels of IL-33 in BAL, possibly due to binding and stabilisation of the soluble cytokine in
126 the absence of DNA binding (Fig 2B). Unexpectedly, when the downstream response to
127 released IL-33 was measured 24 h later (Fig 2C), IL-33 tethering did not correlate with
128 suppression of IL-33-induced responses: while HpARI2 suppressed and HpARI3 amplified
129 eosinophilia, ILC2 activation (as measured by surface CD25 or cell size by median FSC)
130 and IL-5 release (Fig 2D-H), HpARI2:3 could not suppress IL-33 responses despite tethering
131 of IL-33 at the 15 min timepoint (Fig 2B). In fact, HpARI2:3 amplified IL-33-dependent
132 responses similarly to HpARI3, and tended to have increased activity compared to the
133 HpARI3 wild-type protein. Similarly, despite a lack of IL-33 tethering, HpARI3:2 was
134 capable of effectively blocking IL-33 dependent responses similarly to HpARI2 wild-type
135 protein (Fig 2D-H). Therefore, these data indicated that our model of DNA tethering of IL-33
136 by HpARI2 could not fully explain the activity of these proteins.
137
138 We hypothesised that the altered activity of the fusion proteins could be due to their
139 effective half-life in vivo. We administered HpARI2 or HpARI3:2 either 1 day, 3 days or 7
140 days prior to Alternaria (Fig 3A), and found that while HpARI2 could suppress Alternaria-
141 induced eosinophilia and ILC2 responses when administered 3 days prior to allergen,
142 HpARI3:2 could only replicate this suppression when administered 24 h prior to Alternaria
143 (Fig 3B-E, and figure supplement 1-3). Therefore, the in vivo half-life of HpARI2 is controlled
144 by the CCP1 domain, and the HpARI3 CCP1 domain confers a shorter in vivo half-life than
145 the HpARI2 counterpart. As extracellular DNA is only present in the bronchoalveolar lavage
146 at very low concentrations at homeostasis (Curren et al., 2023), and is released in
147 response to stimuli such as Alternaria, we hypothesised that the HpARI2 CCP1 could have
148 a second binding partner which mediates its long in vivo half-life. As other host and
149 pathogen CCP domain proteins have been demonstrated to interact with extracellular
150 matrix constituents such as heparan sulphate (Mark et al., 2006; Schmidt et al., 2008), we
151 hypothesised that this could be the case for the HpARIs also.
152
153 *HpARI2 binds to heparan sulphate*
154 We first used gel filtration chromatography to assess the mobility of HpARIs in the presence
155 or absence of heparan sulphate (HS). While HS addition resulted in earlier elution of
156 HpARI1 and HpARI2, no shift was seen with HpARI3, implying a lack of HS binding (Fig 4A).
157 Likewise, HpARI1 and HpARI2 could be pulled down with heparin-coated beads while
158 HpARI3 could not (Fig 4B). As well as being a common constituent of the extracellular
159 matrix, HS is present on cell surface proteoglycans (Xu & Esko, 2014). To assess whether
160 HS binding could mediate interactions between the HpARIs and stromal cells, we added

PE-conjugated tetramers of the HpARIs to preparations of naïve mouse lung cells, showing that HpARI1 and HpARI2 bind strongly to CD45-negative stromal cells, but less to CD45-positive cells, while HpARI3 did not show detectable binding to any lung cells (Fig 4C). Finally, to assess the respective affinities for HS, we used isothermal calorimetry to show that HpARI1 had an affinity for HS of 9.6 μM, while HpARI2 had a slightly higher affinity of 4.2 μM. Furthermore, these experiments confirmed that no binding could be detected between HpARI3 and HS (Fig 4D-F).

We next used protein modelling to understand the differential heparan sulphate binding of different HpARIs. AlphaFold2 models were produced to predict the structures of the CCP1 domains of HpARI1, HpARI2 and HpARI3. This revealed that while HpARI1 and HpARI2 contain a strongly positively-charged surface, HpARI3 lacks this charged surface (Fig 5A). We next used molecular docking to predict the structure of the complex between HpARI1 or HpARI2 CCP1 domains and the extracellular matrix component heparan sulphate (HS). Docking experiments predicted that HS molecules can dock to various locations across the positive charged surfaces of HpARI1 and HpARI2 CCP1 domains (Fig 5B-C). Therefore, the CCP1 domain of HpARI1 and 2 have a positively-charged surface which acts as a non-specific binding site for negatively charged cellular components, including DNA and heparan sulphates, but this binding surface is lacking in HpARI3.

HpARI2:HS interactions are mediated by CCP1 arginine residues

Electrostatic modelling of HpARI2 indicated that 5 arginine residues in CCP1 form the positively-charged HS and DNA binding surface (Fig 5A). A pentaR mutant of HpARI2 (with each of the indicated Arg resides mutated to Ala) was expressed. HpARI2_pentaR had identical IL-33 suppressive activity in vitro as compared to HpARI2 wild-type (Fig 6A), indicating its IL-33 binding was unaffected. As predicted, however, HpARI2_pentaR lacked binding to both heparin (Fig 6B) and DNA (Fig 6C). When HpARI2_pentaR was administered to mice prior to Alternaria administration, like HpARI3:2, it was found to have a shorter in vivo half-life than the wild-type HpARI2 protein (Fig 6D-H). Taken together, this data shows that HpARI2 is an HS-binding protein, and that interactions with HS increase its in vivo half-life at the site of administration.

Discussion

The parasite helminth *H. polygyrus bakeri* expresses a range of immunomodulatory proteins which have distinct activities. For instance, the TGF-β mimic Hp-TGM binds to the mammalian TGF-β receptor as well as cell surface coreceptors (Johnston et al., 2017; van Dinther et al., 2023). There is a family of 10 Hp-TGM proteins (Hp-TGM1-10) (Smyth et al., 2018) which have distinct activities: HpTGM-1 is an agonist of the TGF-β receptor and uses CD44 as a co-receptor, directing its activity to CD44-positive immune cells such as $CD4^+$ T cells, resulting in regulatory T cell induction (van Dinther et al., 2023). Conversely, in a recent pre-print the related protein Hp-TGM6 was shown to be a TGF-β receptor antagonist which is particularly active on fibroblasts (White et al., 2023), blocking TGF-β signalling. Thus the prototypic Hp-TGM sequence has undergone selection to carry out a range of contradictory functions. Similarly, here we describe the effects of the HpARI family and find that HpARI1 and HpARI2 bind heparan sulphate (HS) and suppress IL-33 responses, while HpARI3 does not bind HS, and amplifies IL-33 responses. As the Hp-TGM proteins are targeted to different cellular targets through co-receptor interactions, we propose that the activity of the HpARIs is controlled by timing of release, in vivo half-life and localisation within the host, controlled by interactions with the extracellular matrix.

We show here that HpARI1 and HpARI2 have a positively charged patch in their CCP1 domain. In the case of HpARI2, we show that this charged patch lengthens the effective half-life of the protein in vivo via binding to DNA and, more relevantly, heparan sulphate. We propose that this binding to the extracellular matrix and cell surface proteoglycans prevents diffusion of HpARI1 and HpARI2, keeps the local concentration high and prevents loss of protein to the circulation. This makes HpARI2 a particularly effective IL-33 suppressor when compared to a systemically administered monoclonal antibody which must reach an effective concentration throughout the circulation of the host to allow blockade at the site of IL-33 release. Some cytokines and chemokines (Ridley et al., 2023) bind to the extracellular matrix to ensure their effects are constrained to the local milieu. This is critical for their activity: it was recently shown that abrogating the HS-binding activity of IFN-γ results in fatal systemic (rather than local) inflammation after viral infection (Kemna et al., 2023). This approach of retaining proteins on the extracellular matrix is being developed for increasing the efficacy of protein-based therapeutics, while decreasing toxicity at off-target sites (Alshoubaki et al., 2023; Martino et al., 2014). This was exemplified in a study showing that heparin binding was able to prolong the blocking of VEGF signalling by recombinant VEGFR1 in therapeutic use (Xin et al., 2021). It appears that this same technique has been evolved by parasitic helminths to localise immunomodulatory proteins. HS binding has been demonstrated for several other CCP domain proteins, including the viral CCP protein Kaposi's sarcoma-associated herpesvirus complement control protein (KCP) (Mark et al., 2006), and the mammalian proteins Factor H (Schmidt et al., 2008) and C4BP (Spijkers et al., 2008; Trouw et al., 2005). In C4BP, the protein presents a basic patch which is able to bind both DNA and HS, similarly to the data we show here for HpARI1 and HpARI2.

While HpARI1 binds to DNA and HS, it has lower affinity for these ligands compared to HpARI2, and in the DNA-binding assays only bound to 50% of the total DNA. It is unclear what the purpose is of this reduced binding affinity, but it could be that HpARI1 remains partially in solution, diffusing further from the site of deposition than HpARI2, and so mediating its effects at a greater distance from the site of release.

In this context, it is interesting that HpARI3 does not bind HS, while having the opposite effect on IL-33 as compared to HpARI2. The effects of IL-33 are highly contingent on the context of IL-33 release, and the cell type and tissue that it is acting on. In parasitic infection, IL-33 released by epithelial cells in the intestine induces a type 2 immune response which results in parasite ejection. In the same helminth infection model, IL-33 released by myeloid cells induced regulatory T cell expansion, suppressing effector immune responses and resulting in increased parasite burdens (Hung et al., 2020). Therefore, at different sites and in different cells, IL-33 can have directly opposing effects.

In the context of the findings outlined here, we propose the following model for the HpARI family's effects: HpARI2 binds strongly to the extracellular matrix, and is retained in the local milieu of the parasite where it blocks IL-33 released in response to infection. HpARI1 binds less strongly to HS, and therefore may diffuse slightly further from the site of deposition, to block more distant IL-33 responses. Finally HpARI3 lacks HS binding and so diffuses freely to amplify IL-33 responses at distal sites, which we hypothesise could amplify IL-33-dependent regulatory responses. To investigate these hypotheses, transgenic parasites deficient for individual HpARI proteins would be useful, however this has proved intractable for parasitic nematodes (Quinzo et al., 2022), and has not been achieved in *H. polygyrus bakeri* to date.

The findings outlined here may be applicable beyond *H. polygyrus bakeri*, as it appears likely that other parasitic helminths have used extracellular matrix binding as a technique to retain immunoregulators within the local milieu. Indeed, *Trichuris muris*, another intestinal nematode, secretes the immunoregulatory protein p43. This protein binds and blocks IL-13, but also has HS binding activity which has been proposed to tether p43 to the extracellular matrix, increasing survival of the protein at the site of infection (Bancroft et al., 2019). *H. polygyrus bakeri* has developed a series of immunomodulatory protein families, including 10 Hp-TGMs and 2 HpBARIs, therefore it will be informative to investigate whether members of these families also bind to the extracellular matrix, and whether this alters their in vivo localisation and/or half-life.

In conclusion, we describe a novel HS-binding ability of members of the HpARI family and show that this binding increases their in vivo half-life and activity at the site of deposition.

Materials and methods

Expression and purification of HpARI proteins and mutants.

Proteins were expressed and purified as described previously (Chauche et al., 2020; Osbourn et al., 2017; Vacca et al., 2020). Briefly, inserts encoding the gene of interest (HpARI1,2,3, HpARI3:2, HpARI2:3 and HpARI_pentaR mutants) were cloned into the pSecTAG2A mammalian expression vector using AscI and NotI-HF restriction enzyme sites, to create constructs encoding these proteins with a C-terminal c-myc epitope tag and 6X-His-tag. These constructs were each transfected into Expi293F cells using the Expifectamine transfection kit (Thermo Fisher Scientific). Cell supernatants were harvested 96 h post-transfection, and the expressed recombinant proteins were then captured from the filtered supernatants using Ni-NTA chromatography, then dialysed to PBS and filter sterilised. The HEK-Blue TLR4 reporter assay (Invivogen) was used to assess endotoxin contamination, and levels of all purified proteins were below the detection limit of the assay (<0.01 EU LPS per µg protein).

Animals

BALB/cAnNCrl and C57BL/6JCrl mice were purchased from Charles River, UK. Experiments were cage blocked: each cage contained one member of each group in the experiment, thus controlling for cage effects. Mouse accommodation and procedures were performed under UK Home Office licenses with institutional oversight performed by qualified veterinarians.

In vivo Alternaria model challenge

BALB/c mice were intranasally administered with 50 µg Alternaria allergen (Greer XPM1D3A25) and 10 µg HpARI wild-type or mutant proteins suspended in PBS, carried out under isoflurane anaesthesia. For most experiments, HpARI proteins and Alternaria allergen were coadministered, but in indicated experiments HpARI proteins were administered 1, 3 or 7 days prior to Alternaria. For IL-33 measurements in BAL, mice were culled 15 min later, and bronchoalveolar lavage (BAL) was collected (one lavage with 0.5 mL ice-cold PBS for cytokine measurements only). IL-33 levels were quantified in undiluted BAL fluid by ELISA following the manufacturer's instructions (R&D systems) and Western Blot using anti-IL-33 antibody (R&D systems). For later immunological response analysis, mice were culled 24 h after Alternaria+HpARI administration, and bronchoalveolar lavage (BAL) was collected (four lavages with 0.5 mL ice-cold PBS for cellular and cytokine measurements). Lungs were taken for single-cell preparation and flow cytometry, as previously described (Colomb et al., 2024; Osbourn et al., 2017). IL-5 levels were quantified in undiluted BAL fluid by ELISA following the manufacturer's instructions (Invitrogen).

Single-cell preparations and flow cytometry

Single cell preparations of lung tissue were prepared as described previously (Osbourn et al., 2017). Lungs were digested by shaking for 35 min at 37ºC in 2U/ml Liberase TL (Sigma) and 80 U/ml DNAseI (Thermo Fisher Scientific) in PBS. Red blood cells in lung and BAL single cell preparations were lysed using ACK buffer, then total viable cell numbers (using trypan blue staining) calculated from haemacytometer cell counts. Cells were stained for viability with Zombie UV Fixable Viability Kit (Biolegend) according to the manufacturer

322 instructions, blocked with anti-mouse CD16/CD32 (clone 93; Biologend) and stained for
323 either ILC2 or eosinophil markers. ILC2 markers: CD45 (AF700, clone 30-F11, or APC-Cy7,
324 I3/2.3; Biolegend), CD90.2 (AF700, clone 30-H12, Biolegend), ICOS (PE, clone C398.4A;
325 Biolegend), lineage markers (all on FITC: CD3ε, clone 145-2C11; CD5, clone 53-7.3;
326 CD11b, clone M1/70.15; CD19, clone 6D5; CD49b, clone DX5; Biolegend), CD25 (PerCP,
327 clone PC61; Biolegend), and ST2 (APC, clone RMST2-2; Invitrogen). Eosinophil markers:
328 CD45 (AF700, clone 30-F11, or APC-Cy7, I3/2.3; Biolegend), SiglecF (PE, clone REA798,
329 Miltenyi), CD11c (AF647, clone N418, Biolegend). Cells were then acquired on a LSR
330 Fortessa (BD) and analyzed on FlowJo v10.9 (BD). Gating strategies and representative flow
331 cytometry plots are shown in Figure 3 - figure supplements 1-3. BAL eosinophils were gated
332 on $SiglecF^{+}CD11c^{-}CD45^{+}$, lung recruited inflammatory eosinophils (Mesnil et al., 2016)
333 were gated on $SiglecF^{hi}CD11c^{-}CD45^{+}$. ILC2s were gated on $ICOS^{+}Lineage^{-}CD45^{+}$ or
334 $ICOS^{+}CD90.2^{+}Lineage^{-}CD45^{+}$ as indicated. Absolute cell numbers were calculated by
335 gating on the population of interest and multiplying the percentage of this population within
336 the live cell gate by the haemacytometer total viable cell count.
337
338 **Electrophoretic mobility shift assays.**
339 IR700-conjugated oligonucleotides were manufactured by Integrated DNA Technologies
340 (IR700-5'-AACTTTGCCATTGTGGAAGG-3', 5'-CCTTCCACAATGCCAAAGTT-3'). 50 fmol of
341 oligonucleotides were incubated in binding buffer (10 mM Tris, 50 mM KCl, 1 mM DTT, 2.5%
342 glycerol, 5 mM $MgCl_2$, 0.05% NP40, pH 7.5) with the indicated concentrations of HpARI
343 proteins for 30 minutes at room temperature. Samples were then run on a 5% gel
344 (Acrylamide/Bisacrylamide 37.5:1 Protogel, National diagnostics) in 0.5% TBE buffer.
345 Images were then acquired on a Licor Odyssey Fc using the IR 700 channel.
346
347 **Heparin-agarose pull-down assays.**
348 Heparin-agarose beads (#H6508, Sigma) were washed twice with PBS 0.02%-tween 20 and
349 incubated with 10 µg of HpARI proteins in a final volume of 100 µL of PBS 0.02%-tween 20.
350 After 30 minutes of incubation at room temperature, the beads were spun down and the
351 supernatant collected. After 3 washes with PBS 0.02% tween 20, the bound fraction was
352 eluted in 1 X Loading Sample Buffer (Thermo Fisher Scientific) containing 5% 2-
353 Mercaptoethanol, heated to 70°C for 5 min and ran on a 4-12% Nupage precast gel (Thermo
354 Fisher Scientific). Protein were then detected using InstantBlue™ Coomassie Stain (Abcam)
355 following manufacturer's instructions.
356
357 **CMT-64 cells culture and treatment.**
358 CMT-64 cells (ECACC 10032301) were maintained in complete RPMI [RPMI 1640 medium
359 containing 10% fetal bovine serum, 2 mM L-glutamine, 100 U/mL penicillin, and 100 µg/mL
360 streptomycin (Thermo Fisher Scientific)] at 37°C, 5% CO_2; 96-well plates were seeded at 5 ×
361 10^4 cells per well. Cells were grown to 100% confluency, washed, and incubated in complete
362 RPMI containing HpARI proteins at the concentrations indicated. Cells were snap frozen on
363 dry ice for at least 1 h, then thawed and incubated at 37°C for 2 h, prior to the collection of
364 supernatants and application to bone marrow cell cultures, as described previously

365 (Colomb et al., 2024).
366
367 **Bone marrow assay and ELISA**
368 Bone marrow single-cell suspensions were prepared from C57BL/6 mice by flushing tibias
369 and femurs with RPMI 1640 medium using a 21 g needle. Cells were resuspended in ACK
370 lysis buffer (Gibco) for 5 min at room temperature, prior to resuspension in complete RPMI
371 (with 10% FCS, 1% penicillin/streptomycin, 1% L-glutamine; Gibco) and passing through a
372 70 µm cell strainer. Cells were cultured in round-bottom 96-well plates in a final 200 µL
373 volume, containing 0.5×10^6 cells/well. IL-2 and IL-7 (Biolegend) were added at a 10 ng/mL
374 final concentration. CMT freeze-thaw supernatant prepared as described earlier was added
375 at 50 µL per well. Cells were then cultured at 37°C, 5% CO_2, for 5 days, prior to supernatant
376 collection. IL-5 concentration was assessed using mouse-uncoated IL-5 enzyme linked
377 immunosorbent assay (ELISA) kits (Invitrogen) following the manufacturer's instructions.
378
379 **Gel Filtration**
380 50 µg of HpARI proteins were incubated with 50 µg of Heparan Sulphate (Heparan sulfate
381 sodium salt from bovine kidney, Sigma) in PBS for 30 min hour at room temperature. The mix
382 was then run through a Superdex 200 Increase 10/300 GL gel filtration column (Cytiva) and
383 detected by monitoring of UV A280nm absorbance.
384
385 **Cell binding assays**
386 HpARI proteins tetramers were prepared by mixing HpARI biotinylated proteins with PE-
387 conjugated streptavidin (Biolegend) at a 4:1 molar ratio for 30 minutes at room temperature.
388 BALB/c mice lungs were taken for single-cell preparation and flow cytometry, as previously
389 described (15). Cells were washed twice in PBS and stained with Zombie UV Fixable Viability
390 Kit (Biolegend) according to the manufacturer instructions. Cells were then incubated for 30
391 min with anti-mouse CD16/CD32 (clone 93; Biolegend) for Fc receptors blocking and then
392 simultaneously incubated with HpARI proteins tetramers and stained for CD45 (APC-Cy7,
393 clone 30-F11; Biolegend). Cells were then acquired on a LSR Fortressa (BD) and analyzed on
394 FlowJo v10.9 (BD).
395
396 **Structural modelling**
397 Full-length models of HpARI1-3 were built using Alphafold with crystal structure of
398 HpARI2_CCP2/3 (PDB ID = 8Q5R) as a template (Tunyasuvunakool et al., 2021). Top-ranking,
399 relaxed Alphafold models were selected for further analysis. Electrostatic potential maps of
400 the HpARI1-3 proteins were generated from the Alphafold model and visualized using
401 Chimera X (Pettersen et al., 2021). The Cluspro server (https://cluspro.org) was used to
402 predict the location of the heparin-binding site on HpARI2. Representative Heparin-HpARI2
403 complex was selected based on scoring criteria described previously (Kozakov et al., 2017).
404
405 **Isothermal Calorimetry**
406 HpARI1, HpARI2 and HpARI3 were first size exclusion chromatography (SEC) purified in a
407 buffer containing 10 mM HEPES pH 7.2 and 100 mM NaCl to remove misfolded protein
408 aggregates. Proteins were then concentrated to 50 µM for isothermal calorimetry

experiments (ITC). All ITC experiments were performed on Microcal PEAQ-ITC (Malvern) and Microcal PEAQ-ITC analysis software was used for data analysis. Direct titration of proteins was done individually against Heparan Sulphate tetrasaccharide (HS4) (Iduron, UK) reconstituted in SEC buffer. Typical titration was carried over 20 injections with an initial injection of 0.4 µl followed by 19 injections of 2 µl of 2 mM Heparan Sulphate tetrasaccharide into protein solution inside the cell, stirring at 750 rpm at room temperature. All titrations were done twice.

Statistics

Statistics Data were analyzed using Graphpad Prism v10.0.0. When comparing independent groups, one-way analysis of variance (ANOVA) with Dunnett's post-test was used. When comparing groups over a timecourse, two-way ANOVA with Dunnett's post-test was used. Standard error of mean is used throughout. $****$ = $P < 0.0001$, $***$ = $P < 0.001$, $**$ = $P < 0.01$, $*$ = $P < 0.05$, ns = not significant ($P > 0.05$).

Acknowledgements

This work was funded by awards to H.J.M. from LONGFONDS|Accelerate as part of the AWWA project, the Medical Research Council (MR/S000593/1), and Wellcome (221914/Z/20/Z).

References

Alshoubaki, Y. K., Lu, Y. Z., Legrand, J. M. D., Karami, R., Fossat, M., Salimova, E., Julier, Z., & Martino, M. M. (2023, May 22). A superior extracellular matrix binding motif to enhance the regenerative activity and safety of therapeutic proteins. *NPJ Regen Med, 8*(1), 25. https://doi.org/10.1038/s41536-023-00297-0

Bancroft, A. J., Levy, C. W., Jowitt, T. A., Hayes, K. S., Thompson, S., McKenzie, E. A., Ball, M. D., Dubaissi, E., France, A. P., Bellina, B., Sharpe, C., Mironov, A., Brown, S. L., Cook, P. C., A, S. M., Thornton, D. J., & Grencis, R. K. (2019, May 28). The major secreted protein of the whipworm parasite tethers to matrix and inhibits interleukin-13 function. *Nat Commun, 10*(1), 2344. https://doi.org/10.1038/s41467-019-09996-z

Bonilla, W. V., Frohlich, A., Senn, K., Kallert, S., Fernandez, M., Johnson, S., Kreutzfeldt, M., Hegazy, A. N., Schrick, C., Fallon, P. G., Klemenz, R., Nakae, S., Adler, H., Merkler, D., Lohning, M., & Pinschewer, D. D. (2012, Feb 24). The alarmin interleukin-33 drives protective antiviral CD8(+) T cell responses. *Science, 335*(6071), 984-989. https://doi.org/10.1126/science.1215418

Chauche, C., Vacca, F., Chia, S. L., Richards, J., Gregory, W. F., Ogunkanbi, A., Wear, M., & McSorley, H. J. (2020). A Truncated Form of HpARI Stabilizes IL-33, Amplifying Responses to the Cytokine. *Front Immunol, 11*, 1363. https://doi.org/10.3389/fimmu.2020.01363

Colomb, F., Ogunkanbi, A., Jamwal, A., Dong, B., Maizels, R. M., Finney, C. A. M., Wasmuth, J. D., Higgins, M. K., & McSorley, H. J. (2024, Mar 12). IL-33-binding HpARI family homologues with divergent effects in suppressing or enhancing type 2 immune responses. *Infect Immun, 92*(3), e0039523. https://doi.org/10.1128/iai.00395-23

Curren, B., Ahmed, T., Howard, D. R., Ashik Ullah, M., Sebina, I., Rashid, R. B., Al Amin Sikder, M., Namubiru, P., Bissell, A., Ngo, S., Jackson, D. J., Toussaint, M., Edwards, M. R., Johnston, S. L., McSorley, H. J., & Phipps, S. (2023, Oct). IL-33-induced neutrophilic inflammation and NETosis underlie rhinovirus-triggered exacerbations of asthma. *Mucosal Immunol, 16*(5), 671-684. https://doi.org/10.1016/j.mucimm.2023.07.002

Hung, L. Y., Tanaka, Y., Herbine, K., Pastore, C., Singh, B., Ferguson, A., Vora, N., Douglas, B., Zullo, K., Behrens, E. M., Li Hui Tan, T., Kohanski, M. A., Bryce, P., Lin, C., Kambayashi, T., Reed, D. R., Brown, B. L., Cohen, N. A., & Herbert, D. R. (2020, Nov 13). Cellular context of IL-33 expression dictates impact on anti-helminth immunity. *Sci Immunol, 5*(53). https://doi.org/10.1126/sciimmunol.abc6259

Jamwal, A., Colomb, F., McSorley, H. J., & Higgins, M. K. (2023). Structural basis for IL-33 recognition and its antagonism by the helminth effector protein HpARI. *bioRxiv*, 2023.2008.2010.552813. https://doi.org/10.1101/2023.08.10.552813

Johnston, C. J. C., Smyth, D. J., Kodali, R. B., White, M. P. J., Harcus, Y., Filbey, K. J., Hewitson, J. P., Hinck, C. S., Ivens, A., Kemter, A. M., Kildemoes, A. O., Le Bihan, T., Soares, D. C., Anderton, S. M., Brenn, T., Wigmore, S. J., Woodcock, H. V., Chambers, R. C., Hinck, A. P., McSorley, H. J., & Maizels, R. M. (2017, Nov 23). A structurally distinct TGF-beta mimic from an intestinal helminth parasite potently induces regulatory T cells. *Nat Commun, 8*(1), 1741. https://doi.org/10.1038/s41467-017-01886-6

Kemna, J., Gout, E., Daniau, L., Lao, J., Weissert, K., Ammann, S., Kuhn, R., Richter, M., Molenda, C., Sporbert, A., Zocholl, D., Klopfleisch, R., Lortat-Jacob, H., Aichele, P., Kammertoens, T., & Blankenstein, T. (2023, Mar). IFNgamma binding to extracellular matrix prevents fatal systemic toxicity. *Nat Immunol, 24*(3), 414-422. https://doi.org/10.1038/s41590-023-01420-5

Kozakov, D., Hall, D. R., Xia, B., Porter, K. A., Padhorny, D., Yueh, C., Beglov, D., & Vajda, S. (2017, Feb). The ClusPro web server for protein-protein docking. *Nat Protoc, 12*(2), 255-278. https://doi.org/10.1038/nprot.2016.169

Maizels, R. M., Smits, H. H., & McSorley, H. J. (2018, Nov 20). Modulation of Host Immunity by Helminths: The Expanding Repertoire of Parasite Effector Molecules. *Immunity, 49*(5), 801-818. https://doi.org/10.1016/j.immuni.2018.10.016

Mark, L., Lee, W. H., Spiller, O. B., Villoutreix, B. O., & Blom, A. M. (2006, Apr). The Kaposi's sarcoma-associated herpesvirus complement control protein (KCP) binds to heparin and cell surfaces via positively charged amino acids in CCP1-2. *Mol Immunol, 43*(10), 1665-1675. https://doi.org/10.1016/j.molimm.2005.09.016

Martino, M. M., Briquez, P. S., Guc, E., Tortelli, F., Kilarski, W. W., Metzger, S., Rice, J. J., Kuhn, G. A., Muller, R., Swartz, M. A., & Hubbell, J. A. (2014, Feb 21). Growth factors engineered for super-affinity to the extracellular matrix enhance tissue healing. *Science, 343*(6173), 885-888. https://doi.org/10.1126/science.1247663

McSorley, H. J., & Smyth, D. J. (2021, Mar). IL-33: A central cytokine in helminth infections. *Semin Immunol, 53*, 101532. https://doi.org/10.1016/j.smim.2021.101532

Mesnil, C., Raulier, S., Paulissen, G., Xiao, X., Birrell, M. A., Pirottin, D., Janss, T., Starkl, P., Ramery, E., Henket, M., Schleich, F. N., Radermecker, M., Thielemans, K., Gillet, L., Thiry, M., Belvisi, M. G., Louis, R., Desmet, C., Marichal, T., & Bureau, F. (2016, Sep 1). Lung-resident eosinophils represent a distinct regulatory eosinophil subset. *J Clin Invest, 126*(9), 3279-3295. https://doi.org/10.1172/JCI85664

Moffatt, M. F., Gut, I. G., Demenais, F., Strachan, D. P., Bouzigon, E., Heath, S., von Mutius, E., Farrall, M., Lathrop, M., Cookson, W., & Consortium, G. (2010, Sep 23). A large-

scale, consortium-based genomewide association study of asthma. *N Engl J Med, 363*(13), 1211-1221. https://doi.org/10.1056/NEJMoa0906312

Oboki, K., Ohno, T., Kajiwara, N., Arae, K., Morita, H., Ishii, A., Nambu, A., Abe, T., Kiyonari, H., Matsumoto, K., Sudo, K., Okumura, K., Saito, H., & Nakae, S. (2010, Oct 26). IL-33 is a crucial amplifier of innate rather than acquired immunity. *Proc Natl Acad Sci U S A, 107*(43), 18581-18586. https://doi.org/10.1073/pnas.1003059107

Osbourn, M., Soares, D. C., Vacca, F., Cohen, E. S., Scott, I. C., Gregory, W. F., Smyth, D. J., Toivakka, M., Kemter, A. M., le Bihan, T., Wear, M., Hoving, D., Filbey, K. J., Hewitson, J. P., Henderson, H., Gonzalez-Ciscar, A., Errington, C., Vermeren, S., Astier, A. L., Wallace, W. A., Schwarze, J., Ivens, A. C., Maizels, R. M., & McSorley, H. J. (2017, Oct 17). HpARI Protein Secreted by a Helminth Parasite Suppresses Interleukin-33. *Immunity, 47*(4), 739-751 e735. https://doi.org/10.1016/j.immuni.2017.09.015

Pettersen, E. F., Goddard, T. D., Huang, C. C., Meng, E. C., Couch, G. S., Croll, T. I., Morris, J. H., & Ferrin, T. E. (2021, Jan). UCSF ChimeraX: Structure visualization for researchers, educators, and developers. *Protein Sci, 30*(1), 70-82. https://doi.org/10.1002/pro.3943

Quinzo, M. J., Perteguer, M. J., Brindley, P. J., Loukas, A., & Sotillo, J. (2022, Mar 28). Transgenesis in parasitic helminths: a brief history and prospects for the future. *Parasit Vectors, 15*(1), 110. https://doi.org/10.1186/s13071-022-05211-z

Ridley, A. J. L., Ou, Y., Karlsson, R., Pun, N., Birchenough, H. L., Mulholland, I. Z., Birch, M. L., MacDonald, A. S., Jowitt, T. A., Lawless, C., Miller, R. L., & Dyer, D. P. (2023, Nov 7). Chemokines form complex signals during inflammation and disease that can be decoded by extracellular matrix proteoglycans. *Sci Signal, 16*(810), eadf2537. https://doi.org/10.1126/scisignal.adf2537

Schiering, C., Krausgruber, T., Chomka, A., Frohlich, A., Adelmann, K., Wohlfert, E. A., Pott, J., Griseri, T., Bollrath, J., Hegazy, A. N., Harrison, O. J., Owens, B. M. J., Lohning, M., Belkaid, Y., Fallon, P. G., & Powrie, F. (2014, Sep 25). The alarmin IL-33 promotes regulatory T-cell function in the intestine. *Nature, 513*(7519), 564-568. https://doi.org/10.1038/nature13577

Schmidt, C. Q., Herbert, A. P., Kavanagh, D., Gandy, C., Fenton, C. J., Blaum, B. S., Lyon, M., Uhrin, D., & Barlow, P. N. (2008, Aug 15). A new map of glycosaminoglycan and C3b binding sites on factor H. *J Immunol, 181*(4), 2610-2619. https://doi.org/10.4049/jimmunol.181.4.2610

Smyth, D. J., Harcus, Y., White, M. P. J., Gregory, W. F., Nahler, J., Stephens, I., Toke-Bjolgerud, E., Hewitson, J. P., Ivens, A., McSorley, H. J., & Maizels, R. M. (2018, Apr). TGF-beta mimic proteins form an extended gene family in the murine parasite

Heligmosomoides polygyrus. *Int J Parasitol, 48*(5), 379-385. https://doi.org/10.1016/j.ijpara.2017.12.004

Spijkers, P. P., Denis, C. V., Blom, A. M., & Lenting, P. J. (2008, Mar). Cellular uptake of C4b-binding protein is mediated by heparan sulfate proteoglycans and CD91/LDL receptor-related protein. *Eur J Immunol, 38*(3), 809-817. https://doi.org/10.1002/eji.200737722

Trouw, L. A., Nilsson, S. C., Goncalves, I., Landberg, G., & Blom, A. M. (2005, Jun 20). C4b-binding protein binds to necrotic cells and DNA, limiting DNA release and inhibiting complement activation. *J Exp Med, 201*(12), 1937-1948. https://doi.org/10.1084/jem.20050189

Tunyasuvunakool, K., Adler, J., Wu, Z., Green, T., Zielinski, M., Zidek, A., Bridgland, A., Cowie, A., Meyer, C., Laydon, A., Velankar, S., Kleywegt, G. J., Bateman, A., Evans, R., Pritzel, A., Figurnov, M., Ronneberger, O., Bates, R., Kohl, S. A. A., Potapenko, A., Ballard, A. J., Romera-Paredes, B., Nikolov, S., Jain, R., Clancy, E., Reiman, D., Petersen, S., Senior, A. W., Kavukcuoglu, K., Birney, E., Kohli, P., Jumper, J., & Hassabis, D. (2021, Aug). Highly accurate protein structure prediction for the human proteome. *Nature, 596*(7873), 590-596. https://doi.org/10.1038/s41586-021-03828-1

Vacca, F., Chauche, C., Jamwal, A., Hinchy, E. C., Heieis, G., Webster, H., Ogunkanbi, A., Sekne, Z., Gregory, W. F., Wear, M., Perona-Wright, G., Higgins, M. K., Nys, J. A., Cohen, E. S., & McSorley, H. J. (2020, May 18). A helminth-derived suppressor of ST2 blocks allergic responses. *Elife, 9*. https://doi.org/10.7554/eLife.54017

van Dinther, M., Cunningham, K. T., Singh, S. P., White, M. P. J., Campion, T., Ciancia, C., van Veelen, P. A., de Ru, A. H., Gonzalez-Prieto, R., Mukundan, A., Byeon, C. H., Staggers, S. R., Hinck, C. S., Hinck, A. P., Dijke, P. T., & Maizels, R. M. (2023, Aug 22). CD44 acts as a coreceptor for cell-specific enhancement of signaling and regulatory T cell induction by TGM1, a parasite TGF-beta mimic. *Proc Natl Acad Sci U S A, 120*(34), e2302370120. https://doi.org/10.1073/pnas.2302370120

White, S. E., Schwartze, T. A., Mukundan, A., Schoenherr, C., Singh, S. P., van Dinther, M., Cunningham, K. T., White, M. P. J., Campion, T., Pritchard, J., Hinck, C. S., Ten Dijke, P., Inman, G., Maizels, R. M., & Hinck, A. P. (2023, Dec 23). TGM6, a helminth secretory product, mimics TGF-beta binding to TbetaRII to antagonize TGF-beta signaling in fibroblasts. *bioRxiv*. https://doi.org/10.1101/2023.12.22.573140

Xin, H., Biswas, N., Li, P., Zhong, C., Chan, T. C., Nudleman, E., & Ferrara, N. (2021, May 25). Heparin-binding VEGFR1 variants as long-acting VEGF inhibitors for treatment of intraocular neovascular disorders. *Proc Natl Acad Sci U S A, 118*(21). https://doi.org/10.1073/pnas.1921252118

Xu, D., & Esko, J. D. (2014). Demystifying heparan sulfate-protein interactions. *Annu Rev Biochem, 83*, 129-157. https://doi.org/10.1146/annurev-biochem-060713-035314

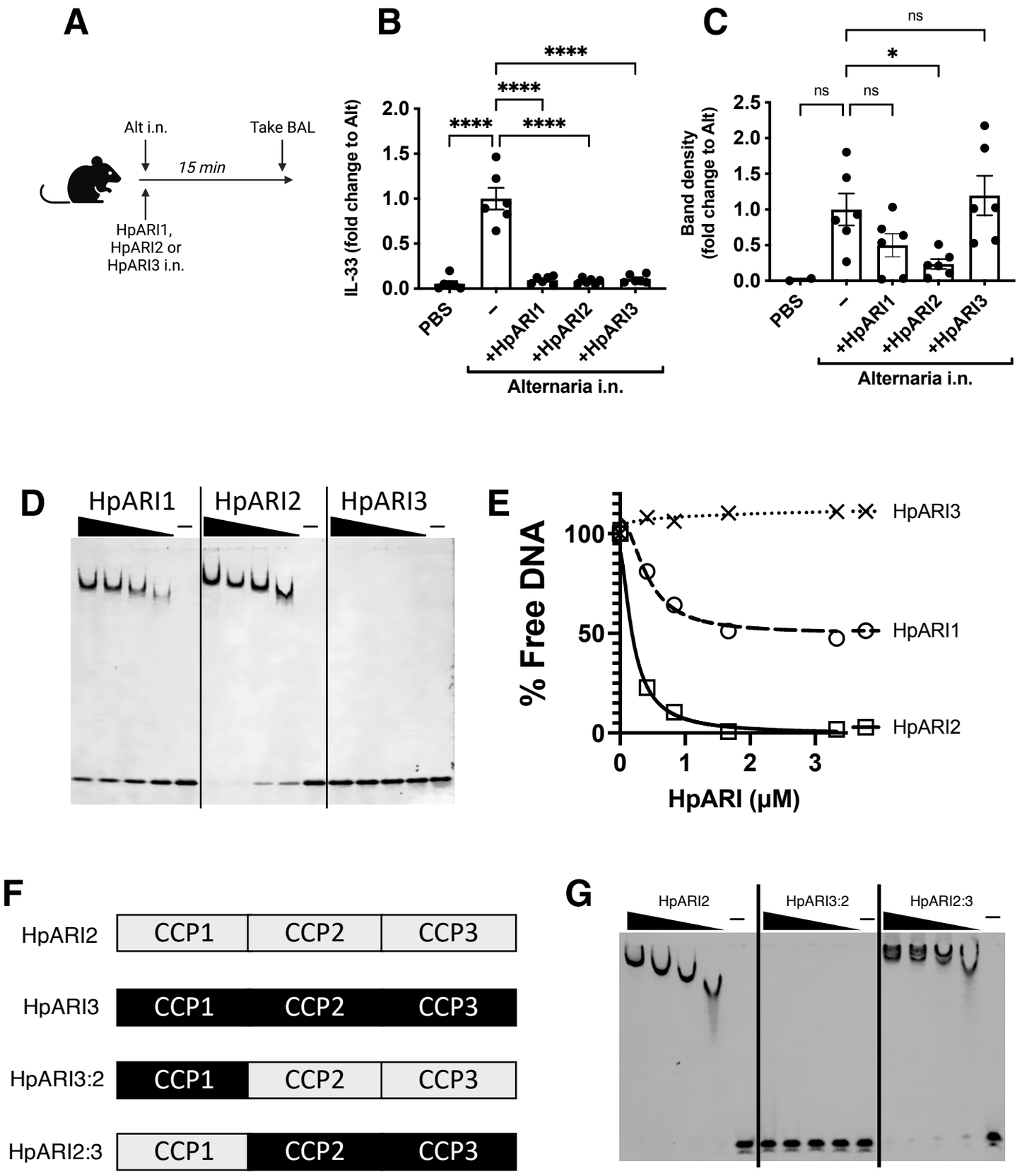

Figure 1: HpARI family members have differing effects against IL-33 release.

A. Experimental setup for B and C.
B. Quantification of mouse IL-33 levels by ELISA in the cell-free BAL fluids of mice treated as shown in A.
C. Quantification of IL-33 by western blot of the samples shown in B.
D. EMSA assay of HpARI1, HpARI2 and HpARI3.
E. Quantification of % free DNA (i.e. low molecular weight band) in the presence of each protein in EMSA assay shown in D.
F. HpARI3:2 and HpARI2:3 fusion protein design.
G. EMSA assay of HpARI2, HpARI3:HpARI2 fusion, or HpARI2:HpARI3 fusion.

Data in B-C pooled from two repeat experiments each with 3 mice per group for a total n=6. Error bar shows SEM. ns = not significant, * = $p<0.05$, **** = $p<0.0001$.

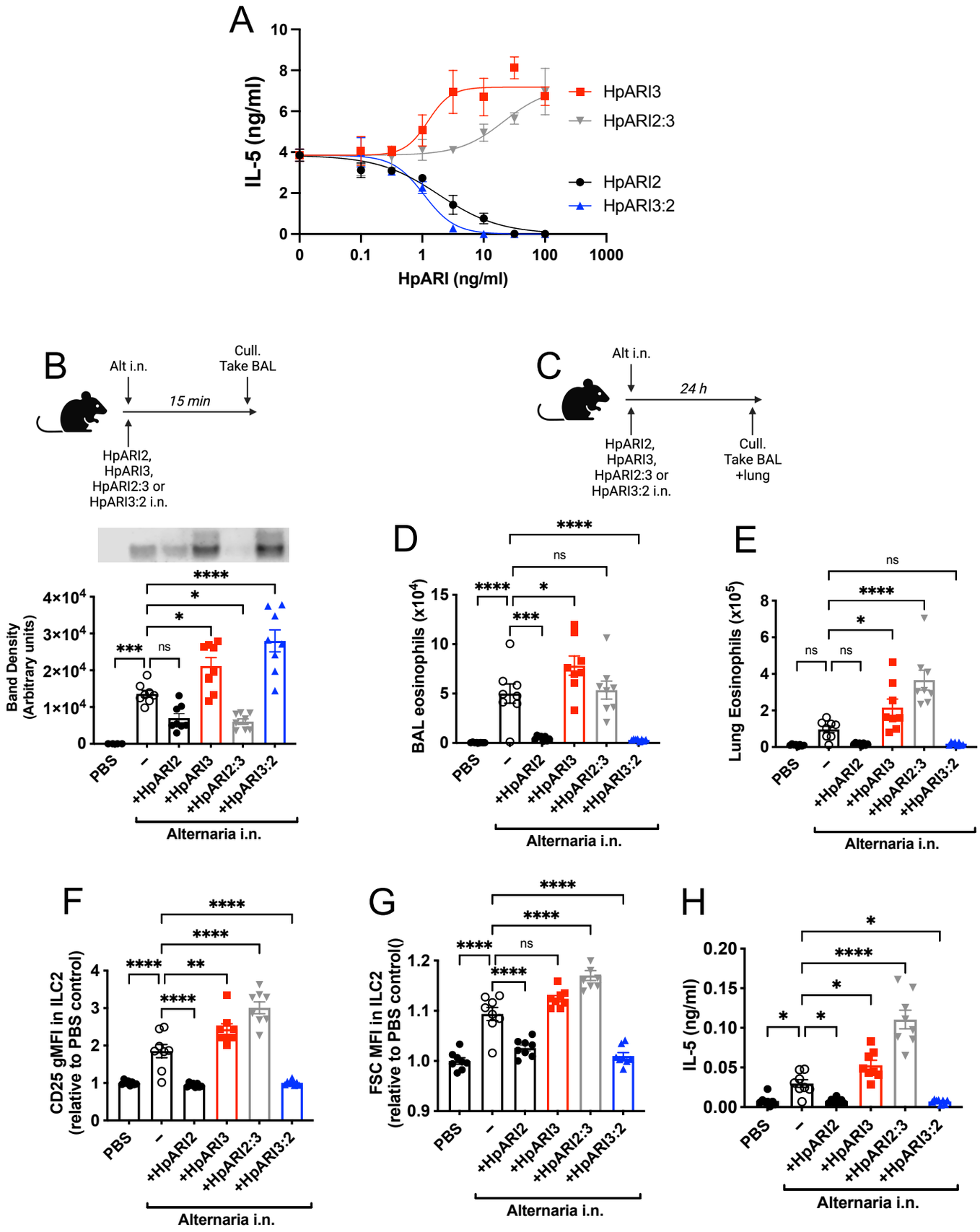

Figure 2: HpARI2:HpARI3 chimeras indicate CCP2/3 domains are central to IL-33 amplification versus suppression.

A. IL-5 production from bone marrow cells in response to IL-2, IL-7 and freeze-thawed CMT-64 supernatants, in the presence of range of concentrations of HpARI2, HpARI3, HpARI2:3 or HpARI3:2. Data pooled from 3 biological replicates.
B. Alternaria allergen with HpARI2, HpARI3 or fusions were administered to mice, cell-free BAL fluid prepared 15 min later, and IL-33 measured by western blot.
C. Experimental set up for D-H.
D. BAL eosinophil numbers (Siglecf^{+}CD11^{-}CD45^{+}) from mice treated as shown in B.
E. Eosinophil (Siglecf^{hi}CD11^{-}CD45^{+}) numbers in lung tissue from mice treated as shown in B.
F. CD25 expression level on lung ILC2 (ICOS^{+}Lin^{-}CD45^{+}) from mice treated as shown in B.
G. FSC mean in lung ILC2 (ICOS^{+}Lin^{-}CD45^{+}) from mice treated as shown in B.
H. BAL IL-5 levels (ELISA) from mice treated as shown in B.

All in vivo data pooled from two repeat experiments each with 4 mice per group for a total n=8. Error bar shows SEM. NS= not significant, *= $p<0.05$ ** = $p<0.01$, *** = $p<0.001$, **** = $p<0.0001$.

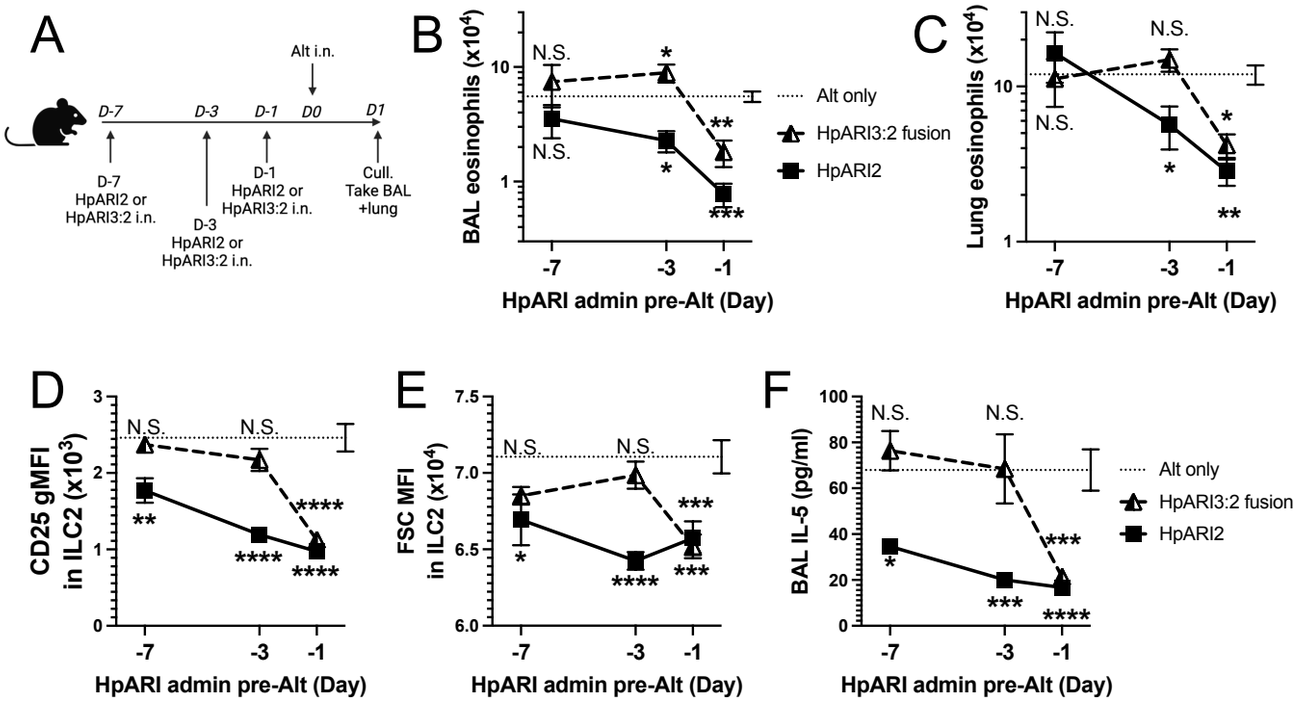

Figure 3: HpARI fusion proteins show CCP1 domain determines half-life in vivo.

A. Experimental setup for B-E. HpARI2 or HpARI3:2 fusion were administered intranasally 7, 3 or 1 day prior to Alternaria allergen. Mice were culled 24 h after Alternaria administration, and BAL and lung tissue taken for analysis.
B. BAL eosinophil numbers (Siglecf^{+}CD11^{-}CD45^{+}) from mice treated as shown in A.
C. Eosinophil (Siglecf^{hi}CD11^{-}CD45^{+}) numbers in lung tissue from mice treated as shown in A.
D. CD25 geometric mean fluorescence intensity on lung ILC2 (ICOS^{+}CD90^{+}Lin^{-}CD45^{+}) from mice treated as shown in A.
E. FSC mean in lung ILC2 from mice treated as shown in A.
F. BAL IL-5 levels (ELISA) from mice treated as shown in A.

Data from day -7 timepoint from a single experimental repeat, all other groups pooled from 2 experiments. Total biological repeats at day 7 = 4, all other timepoints n=8. Error bar shows SEM. NS= not significant, *= $p<0.05$ ** = $p<0.01$, *** = $p<0.001$, **** = $p<0.0001$. Analysed by 2 way ANOVA with Dunnet's post test.

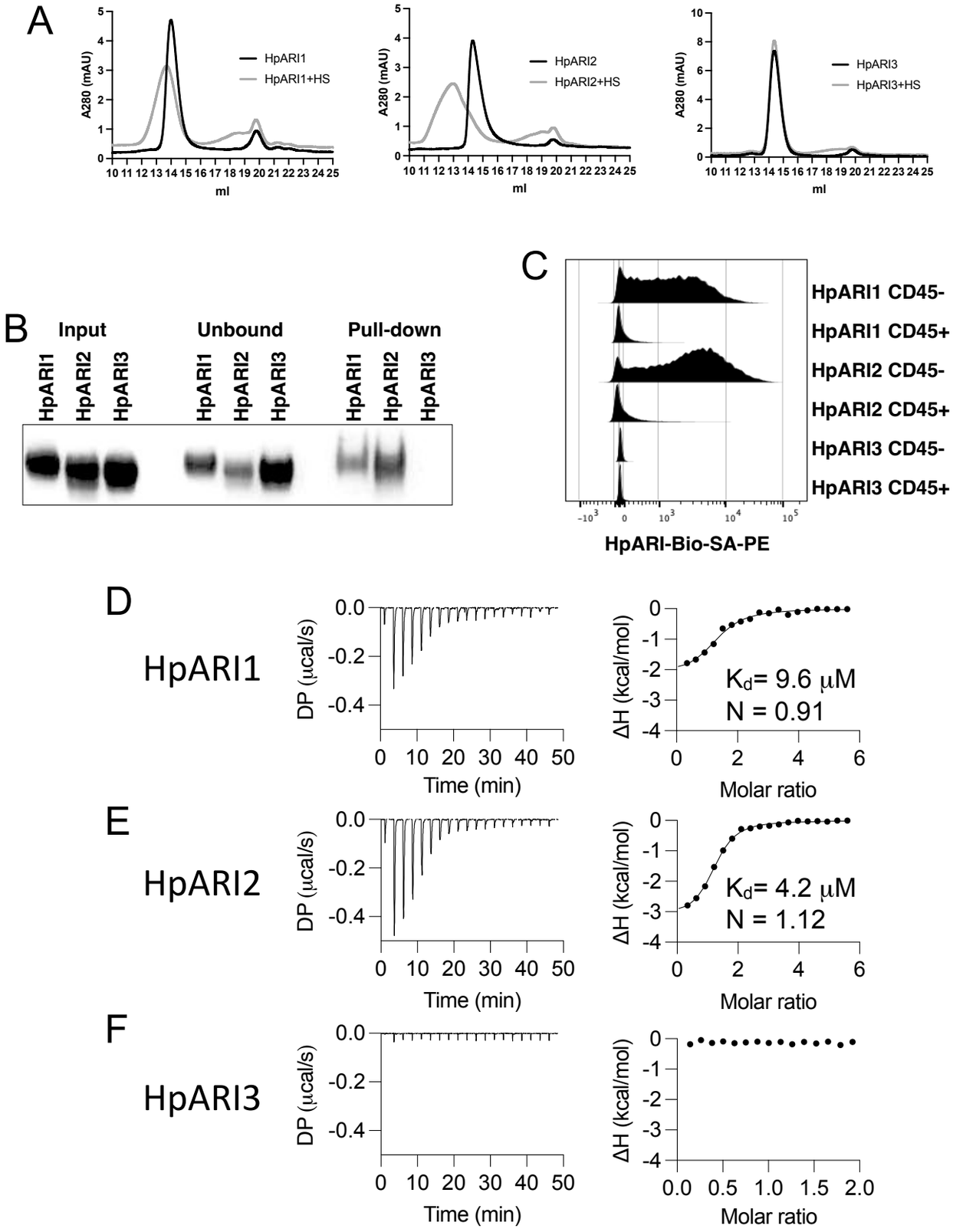

Figure 4: HpARI proteins have variable levels of heparin sulphate binding.

A. 50 µg of HpARI1, HpARI2 or HpARI3 were added to 50 µg Heparin Sulphate (HS) and ran on a Superdex 200 Increase 10/300 GL gel filtration column. A280 trace shown.

B. Coomassie gel of HpARI1, HpARI2 or HpARI3 pull down using HS-coated beads. Input, unbound (ie supernatant from beads) and pull-down elution shown. Representative of 3 repeat experiments.

C. Flow cytometry staining of HpARI1, HpARI2 or HpARI3 tetramers with streptavidin-PE, on naive mouse lung cells gated on live CD45+ or live CD45- cells. Representatives 2 repeat experiments.

D. Isothermal calorimetry of HpARI1 +/- HS

E. Isothermal calorimetry of HpARI2 +/- HS

F. Isothermal calorimetry of HpARI3 +/- HS

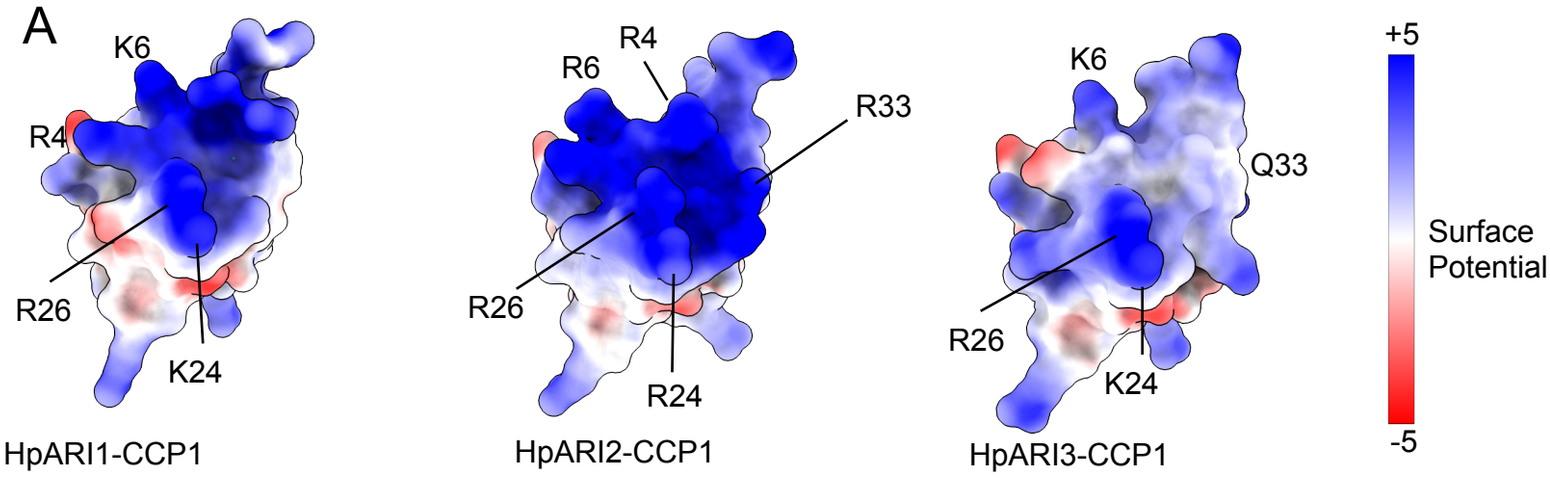


```
HpARI1   1 ANLRCKFTDEERDKGYTGMLVNGKERKAARNGTTVELICGRGNHNYTCTSGHLTANSLRQERCG 60
HpARI2   1 AGQRCRFTDVERDKGYTGMLLKGRLRKTAGNGRTVELICGRGNHQYTCESGVLKESSPRQARCG 60
HpARI3   1 ASLGCKFTDVEKDKGYTGMLVGGKRRESAANGQKVELVCGRGNHNYTCKSGILTEESYRQGRCG 60
           *.  *:*** *:********: *: *::* ** .***:******:*** ** *. .* ** ***
```

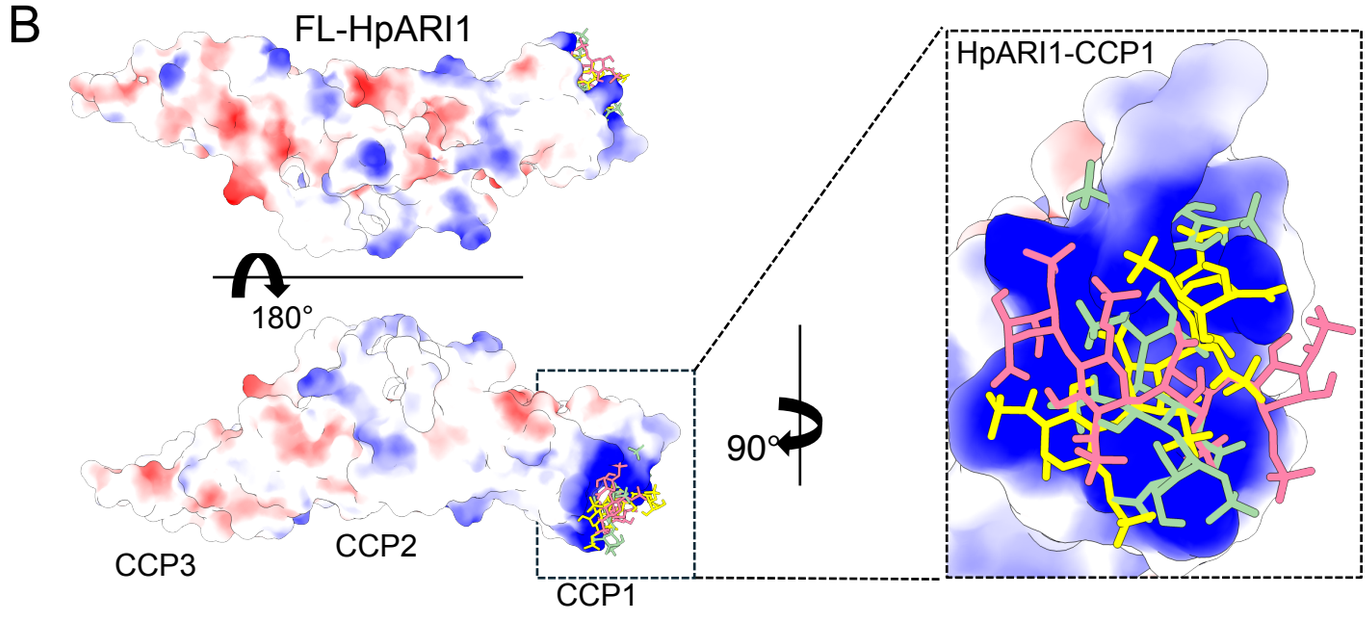

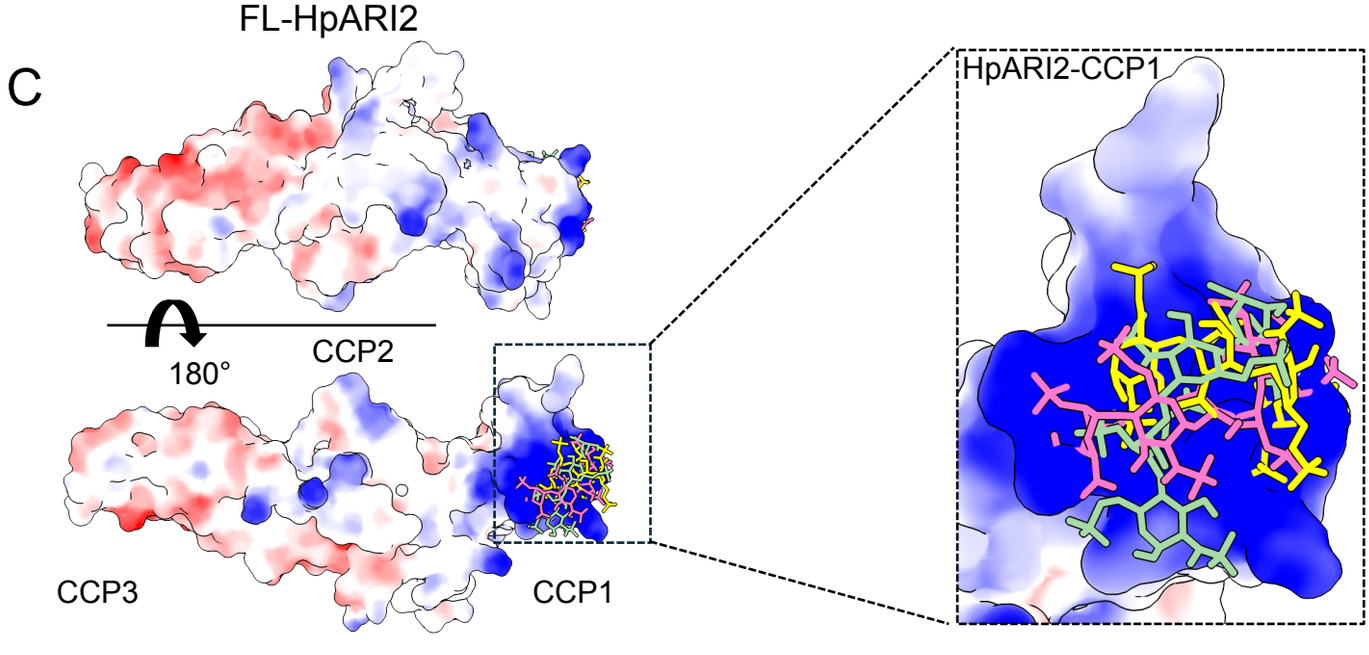

Figure 5: Molecular modelling of HpARI2 interaction of Heparin oligosaccharide.
A. The top panel shows electrostatic surface rendering of alpha fold models of the CCP1 domains of HpARI1-3. Blue and red surfaces indicate positive and negative surfaces respectively. The lower panel shows an amino acid sequence alignment of HpARI family proteins with residues contributing to electropositive patch highlighted in cyan.
B and C. Electrostatic surface representation of an AlphaFold model of heparin tetrasaccharide docked on full-length HpARI1 (B) and HpARI2 (C). Three different docking solutions are shown. The right-hand panels show the spread of these models with heparins shown as coloured sticks on a surface representation of the CCP1 domain.

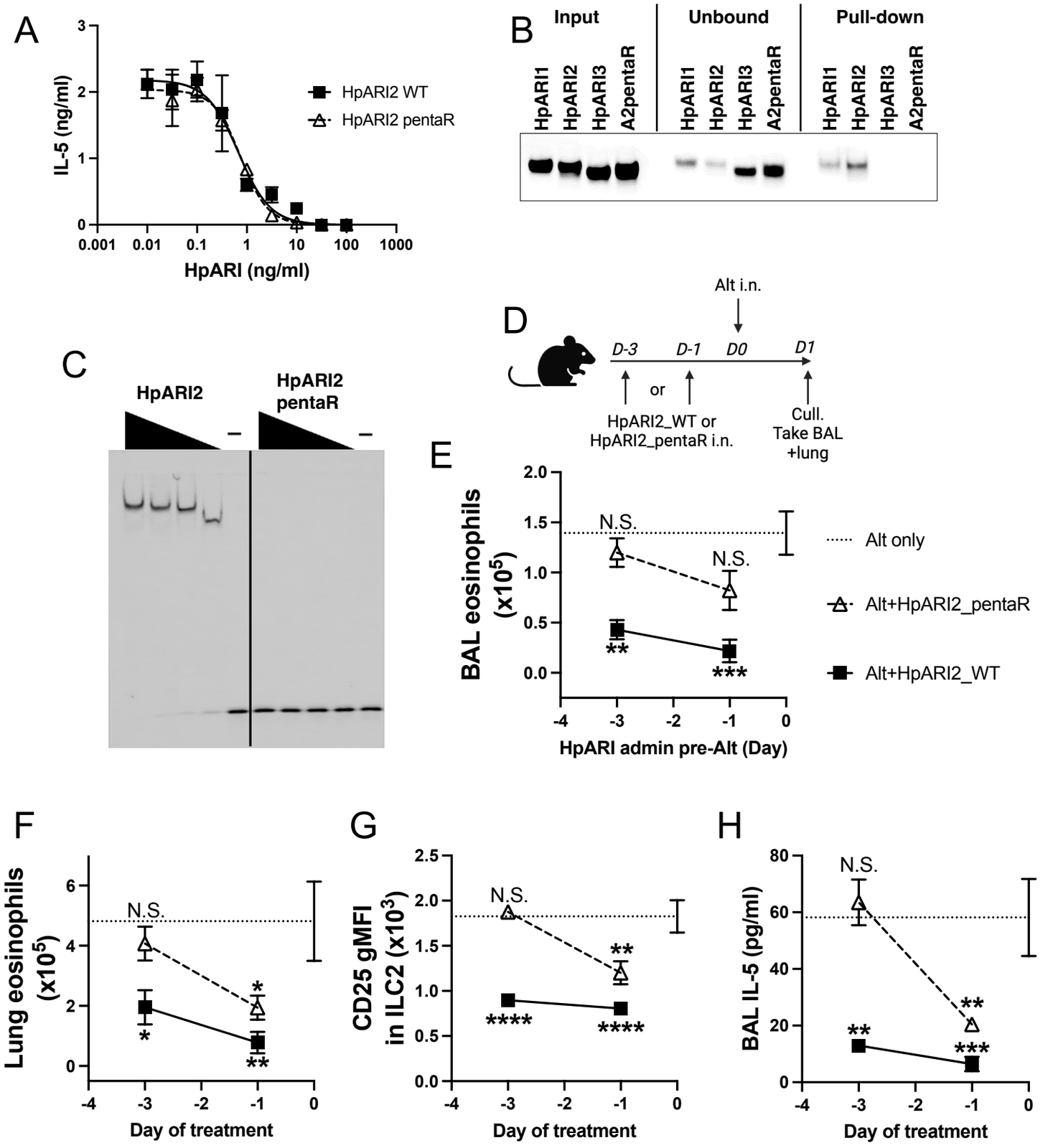

Figure 6: HpARI2 pentaR mutant effectively blocks IL-33 responses in vitro, but has a short half-life in vivo.

A. IL-5 production from bone marrow cells in response to IL-2, IL-7 and freeze-thawed CMT-64 supernatants, in the presence of range of concentrations of HpARI2_WT or HpARI2_pentaR. Data pooled from 3 biological replicates.
B. Coomassie gel of HpARI1, HpARI2, HpARI3 or HpARI2-pentaR (A2pentaR) pull down using heparin-coated beads. Input, unbound (ie supernatant from beads) and pull-down elution shown. Representative of 3 repeats.
C. EMSA assay of HpARI2 or HpARI2_pentaR. Representative of 2 repeats.
D. Experimental setup for C-F. HpARI2_WT or HpARI2_pentaR (10 µg of each) were administered intranasally 3 days or 1 day prior to Alternaria (Alt) allergen. Mice were culled 24 h after Alternaria administration, and BAL and lung tissue taken for analysis.
E. BAL eosinophil numbers (Siglecf^{+}CD11^{-}CD45^{+}) from mice treated as shown in B.
F. Eosinophil (Siglecf^{hi}CD11^{-}CD45^{+}) numbers in lung tissue from mice treated as shown in B.
G. CD25 geometric mean fluorescence intensity on lung ILC2 (ICOS^{+}Lin^{-}CD45^{+}) from mice treated as shown in B.
H. BAL IL-5 levels (ELISA) from mice treated as shown in B.

Data in E-H from a single experiment, for a total of 4 biological replicates per timepoint. Error bar shows SEM. NS= not significant, *= $p<0.05$ ** = $p<0.01$, *** = $p<0.001$, **** = $p<0.0001$. Analysed by 1 way ANOVA with Dunnet's post test, comparing each condition to Alternaria-only control.

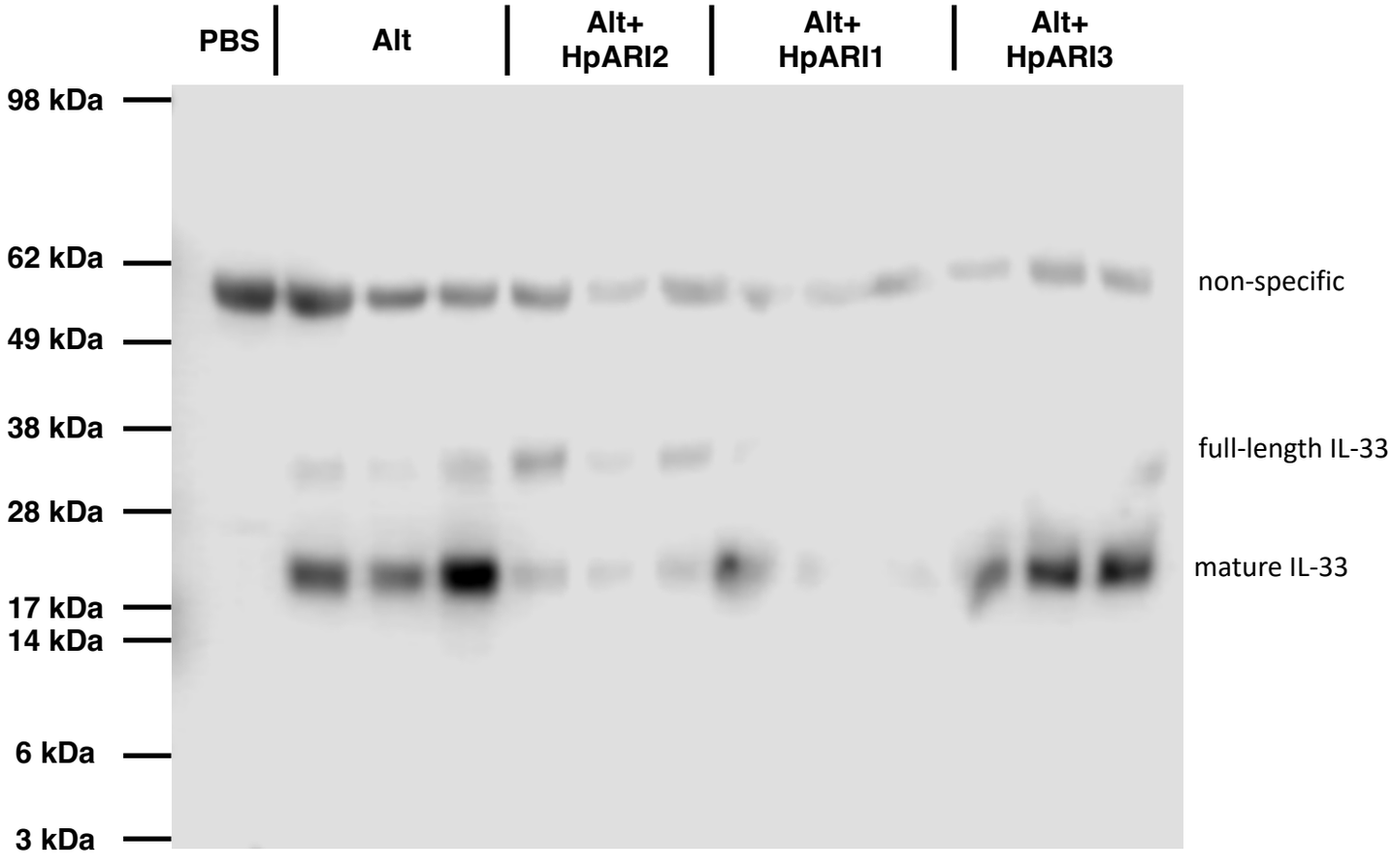

Figure 1 - figure supplement 1: IL-33 western blot in BAL supernatant.
Western blot for IL-33 in BAL supernatant. Mature IL-33 band at ~18 kDa used for densitometry measurements shown in Fig 1C. Representative of 2 repeat experiments, data from both experiments pooled in Fig 1C.

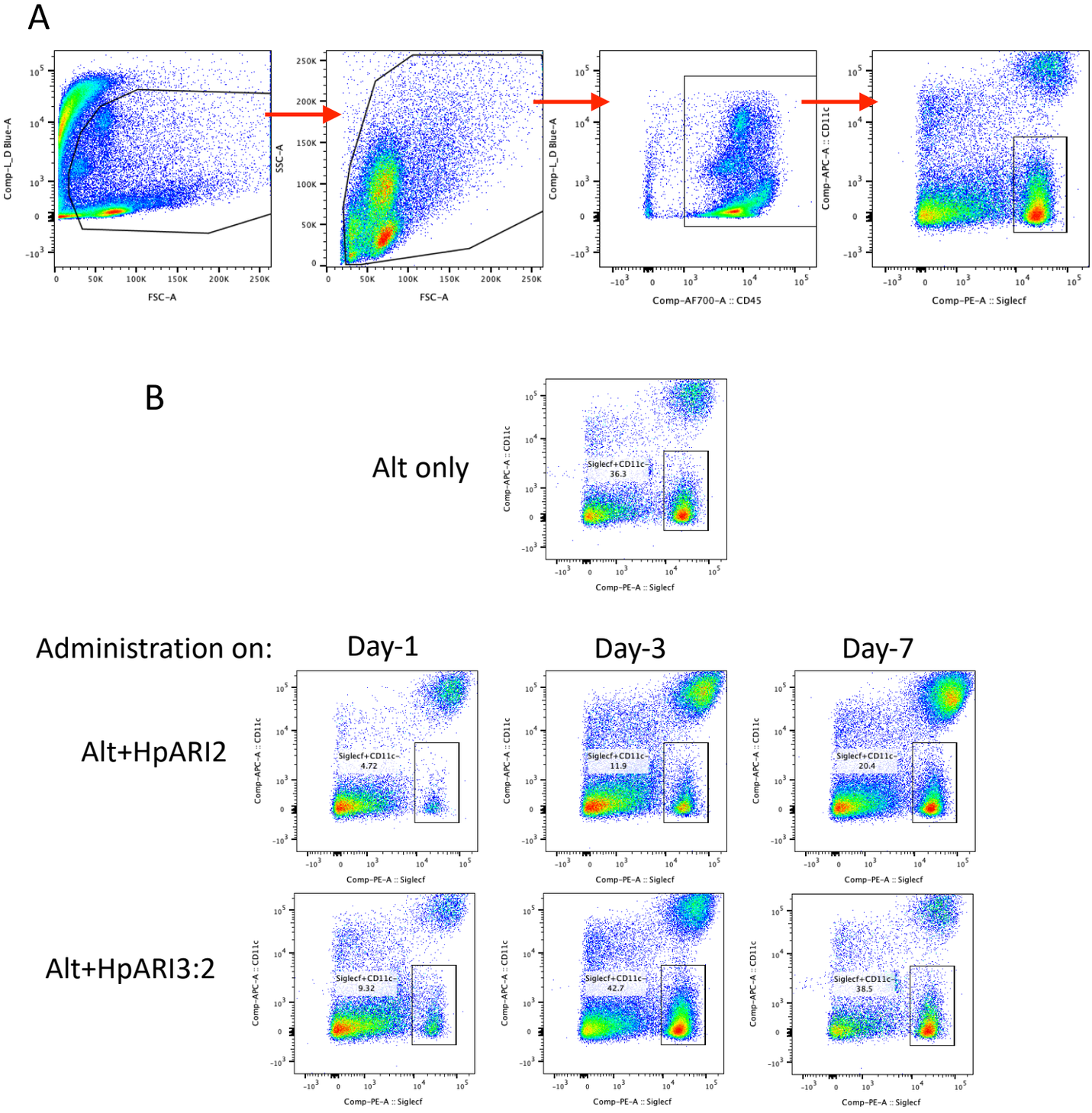

Figure 3 - figure supplement 1: Gating strategy and representative flow plots for bronchoalveolar lavage (BAL) eosinophils

A. Gating strategy for BAL cells. Cells were gated on FSC versus zombie UV viability stain to exclude debris and dead cells, then gated for all cells by FSC versus SSC, then on CD45-positive cells, and finally for SiglecF^{+}CD11c^{-} eosinophils.

B. Representative flow cytometry plots for BAL SiglecF^{+}CD11c^{-} eosinophils, gated on live CD45^{+} cells, as shown in (A). Data used to calculate total BAL eosinophil cell numbers shown in Figure 3B.

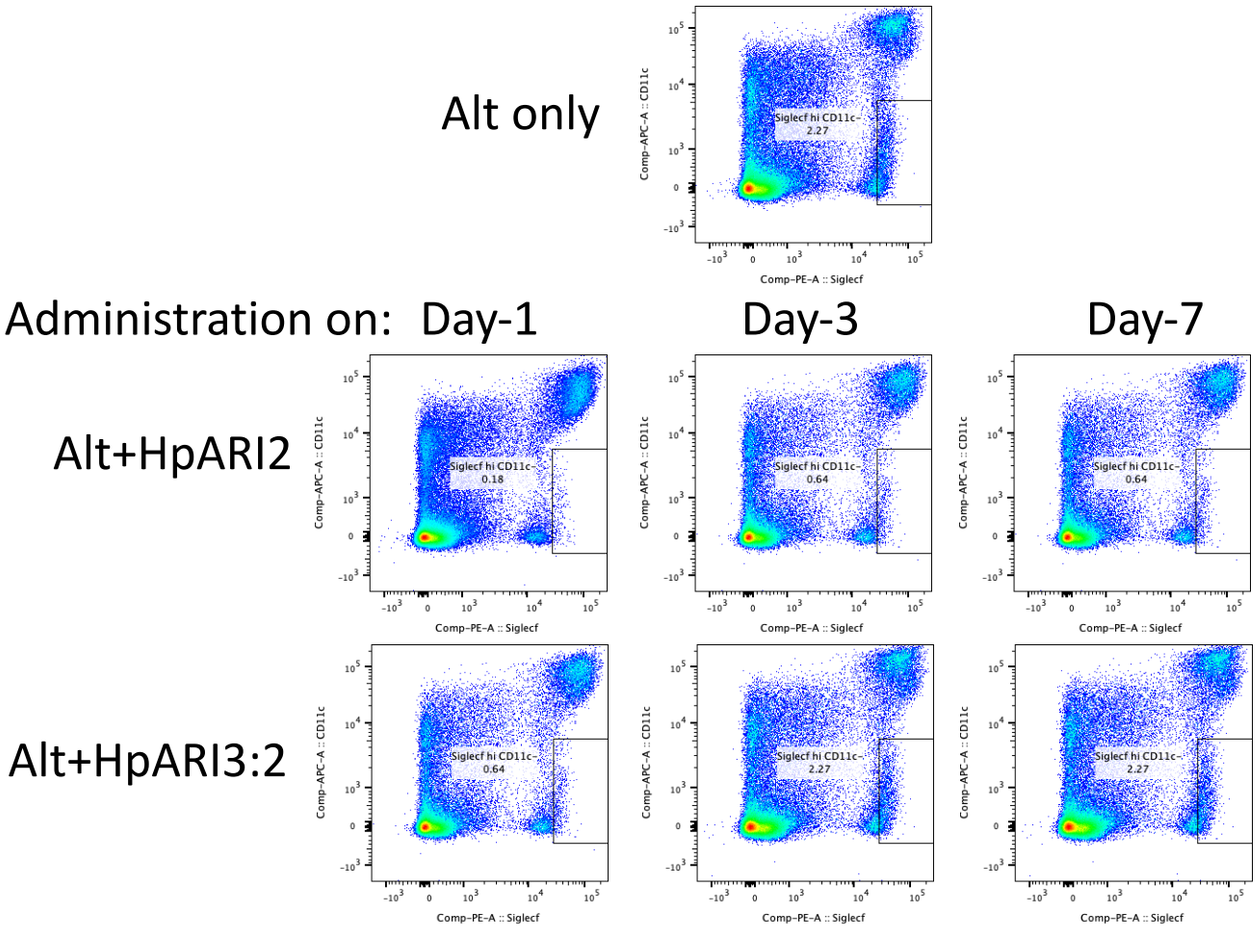

Figure 3 - figure supplement 2: Representative flow plots for lung tissue cells
Representative flow cytometry plots for lung SiglecF^{hi}CD11c^{-} eosinophils, gated on live CD45-positive cells. Data shown here was used to calculate total lung eosinophil cell numbers shown in Figure 3C.

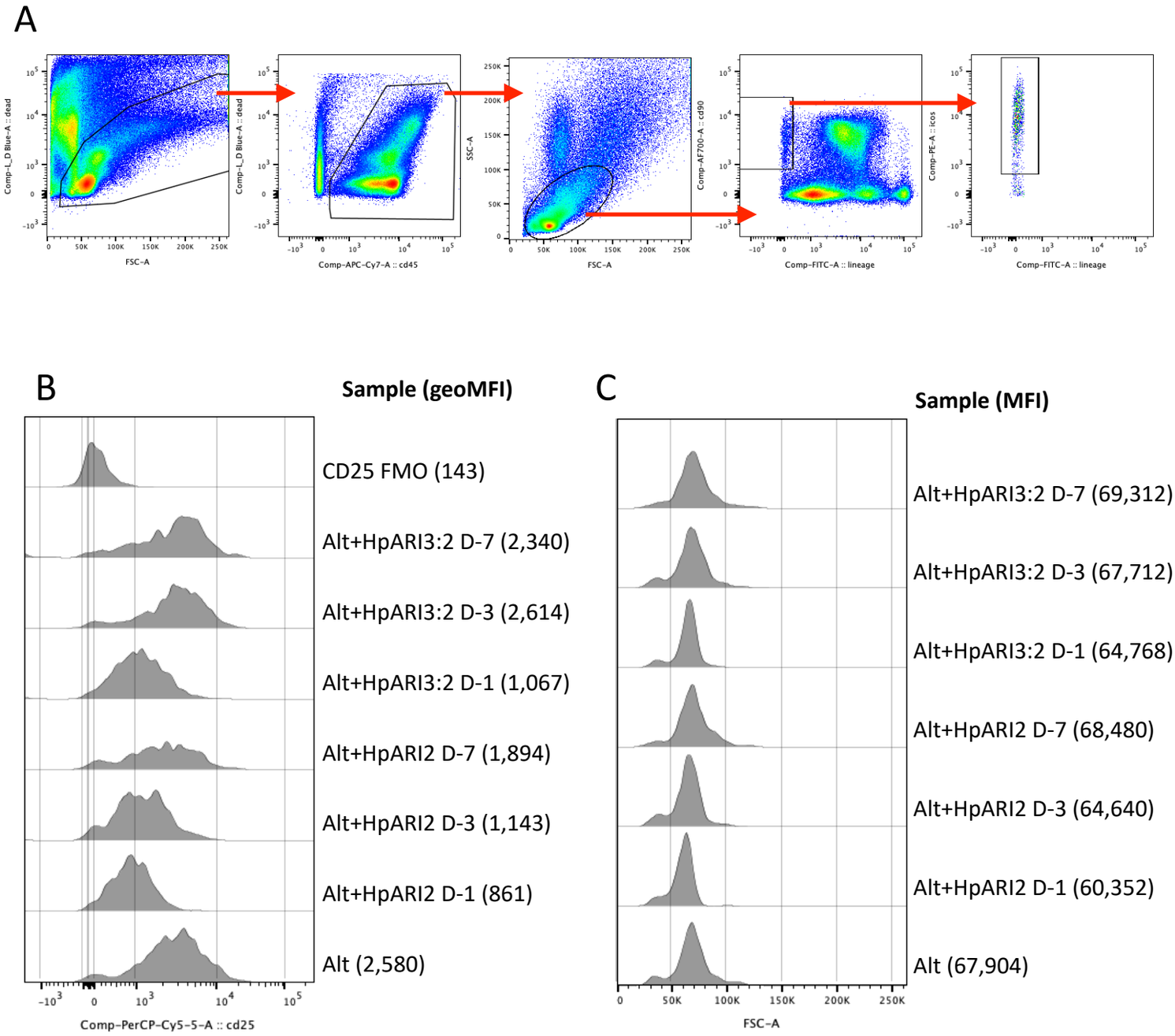

Figure 3 - figure supplement 3: Gating strategy and representative flow plots for lung tissue type 2 innate lymphoid cells (ILC2)

A. Gating strategy for lung ILC2s. Cells were gated on FSC versus zombie UV viability stain to exclude debris and dead cells, then on CD45-positive cells, lymphocytes by FSC versus SSC, and finally for CD90.2^{+}ICOS^{+}Lineage^{-} ILC2s.

B. Representative histograms for CD25 expression in gated ILC2s. Samples representative of data shown in Figure 3C. Geometric Mean Fluorescence Intensity (GeoMFI) shown in brackets. CD25 fluorescence minus one (FMO) control also shown.

C. Representative histograms for FSC signal in gated ILC2s. Samples representative of data shown in Figure 3D. Median Fluorescence Intensity (MFI) shown in brackets.